Journal of Materials Chemistry C

PAPER

View Article Online
View Journal | View Issue

A systematic study of the atmospheric pressure growth of large-area hexagonal crystalline boron nitride film

Cite this: J. Mater. Chem. C, 2014, 2, 1650

Roland Yingjie Tay,[ab] Xingli Wang,[a] Siu Hon Tsang,[b] Guan Chee Loh,[cd] Ram Sevak Singh,[a] Hong Li,[a] Govind Mallick[be] and Edwin Hang Tong Teo*[af]

Received 11th October 2013
Accepted 17th November 2013

DOI: 10.1039/c3tc32011a

www.rsc.org/MaterialsC

The growth of hexagonal boron nitride (h-BN) is of much interest owing to its outstanding properties and for scalable two dimensional (2D) electronics applications. Here, we report the controllable growth of h-BN on a copper substrate using the atmospheric pressure chemical vapor deposition (APCVD) method using ammonia borane as the precursor. The advantages of using APCVD include its ease of setup utilizing fewer resources, low cost and fast growth, all of which are essential for full film coverage and the mass production of 2D h-BN. In this study, we observed a substrate-position dependent evolution of h-BN domains at various stages of growth as the density and size of the domains increased downstream along the quartz tube. Other critical parameters such as growth temperature, deposition time, temperature and mass of precursor were also systemically investigated in order to understand the factors influencing the growth of the h-BN film. Importantly, with a slight increase in the growth temperature of 50 °C, we observe a significant (~17-fold) increase in the average domain size, and its further expansion for a longer duration of growth. Likewise, our parametric study highlights the impact of other crucial parameters on domain size, coverage, and thickness of the h-BN film.

Introduction

Hexagonal boron nitride (h-BN), known colloquially as 'white graphene', has many similar properties to graphene. In a monolayer basal h-BN plane, alternate boron and nitrogen atoms are bonded in a hexagonal manner with sp^2 hybridization. The B–N bonds within each layer are strong covalent bonds. However, the planar layers are bonded by relatively weak Van der Waals forces, giving rise to facile exfoliation. h-BN is an electrical insulator with a wide bandgap (~6 eV),[1] it has high thermal stability (1000 °C),[2] and very high thermal conductivity (2000 W mk^{-1}).[3] It is chemically inert, resistant to corrosion, atomically smooth (free from dangling bonds and trapped charges),[4,5] and possesses high mechanical strength and hardness.[2] These exceptional properties make h-BN useful for many applications such as for use as a lasing material in the ultraviolet spectrum,[1] a potential dielectric support for graphene[4–6] (its lattice constant almost matches that of graphene ~0.25 nm),[7] protective coatings,[8,9] a heat spreader, and a thermal interface material.[10] Ultrathin h-BN has been used as a promising tunneling barrier in field-effect tunneling transistors,[11] and it could also be used as an efficient passivating dielectric layer in solar cell[12,13] devices. In the context of all the interesting applications above, the production of large-area and high quality continuous films of h-BN is in demand.

A few methods have been reported to obtain monolayer or few-layer h-BN either by top-down or bottom-up approaches. Top-down mechanical cleavage was executed using scotch tape,[14] also known as exfoliation, and the bottom-up approach was achieved by ball milling.[15] Few-layer h-BN flakes can also be exfoliated by ultra-sonication and centrifugation through a solution, which is also known as liquid phase exfoliation.[16,17] However, the flakes were reported to be small (<10 μm in length), with random thicknesses and low yields. Recently, the synthesis of h-BN by chemical vapor deposition (CVD) has gained popularity as it promises high yields and better quality manufacturing.[6,18–23] Generally, different sizes of h-BN domains and film thicknesses can be obtained by varying parameters such as the mass and temperature of the precursor and/or the growth time and pressure of the CVD system.[19–21] Both low pressure (LP) and atmospheric pressure (AP) CVD have been used to synthesize h-BN. However, due to evaporation, the

[a]School of Electrical and Electronic Engineering, Nanyang Technological University, 50 Nanyang Avenue, Singapore 639798, Singapore. E-mail: HTTEO@ntu.edu.sg; Tel: +65 6790 6371
[b]Temasek Laboratories@NTU, 50 Nanyang Avenue, Singapore 639798, Singapore
[c]Institute of High Performance Computing, 1 Fusionopolis Way, #16-16 Connexis, Singapore 138632
[d]Department of Physics, Michigan Technological University, Houghton, Michigan 49931, USA
[e]Weapons and Materials Research Directorate, U.S. Army Research Laboratory, Aberdeen Proving Ground, MD, 21005, USA
[f]School of Materials Science and Engineering, Nanyang Technological University, 50 Nanyang Avenue, Singapore 639798, Singapore

copper substrates tend to deform at high temperatures in LPCVD,[24] resulting in lower quality products. On the other hand, APCVD utilizes fewer resources, has a lower operating cost, and is generally simpler in design, making it a preferred fabrication technique for an easy transition into industries. As such, this report aims to give a better understanding of the growth mechanism of h-BN under APCVD conditions on Cu substrates by systematically studying various crucial growth parameters.

Experimental section

Growth of h-BN films

The growth of h-BN films was carried out in a split tube furnace using 25 μm thick Cu substrates purchased from Alfa Aesar (product no. 13382) as catalysts.[18] In our work, however, the general experimental setup was slightly tweaked as shown in the schematic layout in Fig. 1. The precursor ammonia borane (H_3NBH_3), purchased from Sigma Aldrich, was placed 25 cm away from a (2×15) cm^2 Cu substrate in the furnace. Prior to deposition, the Cu was dipped into dilute nitric acid and rinsed in DI water. The substrate was divided into four regions (A to D) and each region was further sub-divided into three regions (1–3). The annealing of the sample comprises two main steps: (i) 800 °C for 20 min in Ar/H_2 (425 : 75 sccm) and (ii) gradual heating up to 1050 °C for 40 min. During the growth process, the temperature was kept at 1050 °C for 30 min and gas flow of Ar/H_2 was decreased to 170 : 30 sccm. Initially, 5 mg of ammonia borane was placed in a ceramic holder within the quartz tube and was heated at 60 °C with a flexible heating belt.

Transfer process

The h-BN film was transferred onto 285 nm SiO_2/Si and quartz substrates by the poly(methyl methacrylate) (PMMA) method.[25] A layer of PMMA was first coated on top of the Cu substrate at 3000 rpm for 30 s, and $Fe(NO_3)_3$ was used to etch away the Cu. The free standing PMMA coated h-BN was then rinsed in DI water several times and extracted onto the SiO_2/Si or quartz substrate. Finally, the sample was submerged in acetone to remove the PMMA.

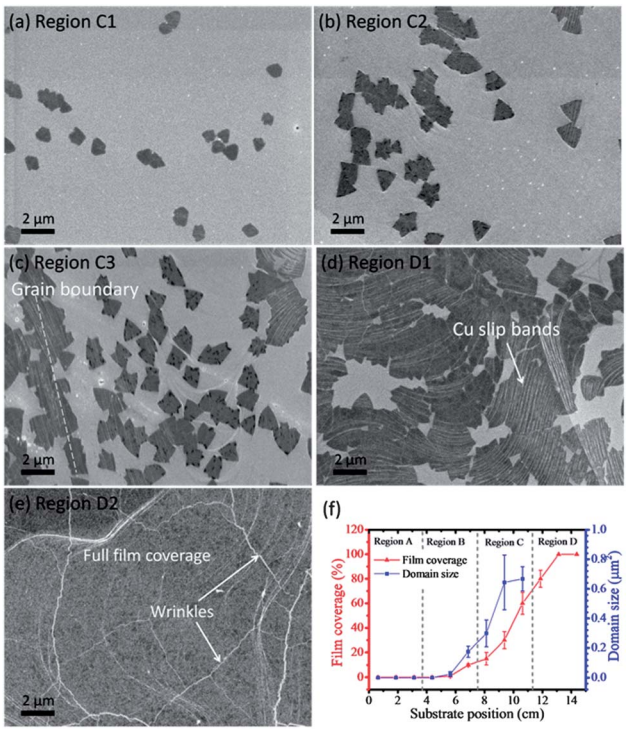

Fig. 2 SEM images of the as-grown BN film on Cu after 30 min of growth time at (a) region C1, (b) region C2, (c) region C3, (d) region D1, (e) region D2, and (f) plots showing substrate-position-dependent film coverage (red) and size of triangular h-BN domains (blue).

Characterization of h-BN films

The formation of h-BN films under the different conditions was investigated using scanning electron microscopy (SEM; LEO 1550 Gemini). Raman spectroscopy (WITec) with a laser excitation wavelength of 532 nm was used at room temperature to further confirm the unique signature of the as-grown h-BN film. The film morphology, thickness and uniformity were monitored with atomic force microscopy (AFM) (Cypher scanning probe microscopy). Ultraviolet visible (UV-vis) spectroscopy (Shimadzu UV-2450) was used to measure the optical bandgap (OBG) of the h-BN film.

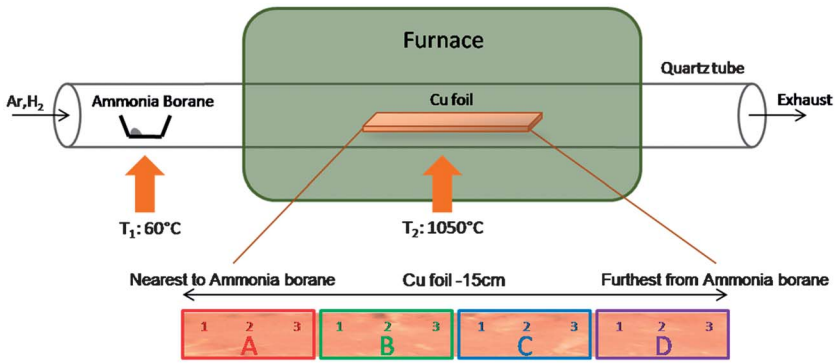

Fig. 1 Schematic layout of the CVD system. Regions A–D are the respective positions on the Cu substrate with 1–3 as the sub divisions within each defined region.

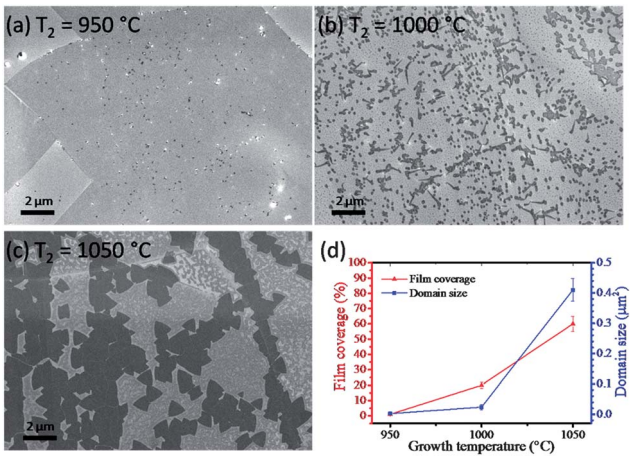

Fig. 3 Dependence of the h-BN domains at various growth temperatures (T_2). SEM images of the as-grown BN films on Cu after 10 min of deposition with growth temperatures at (a) 950 °C, (b) 1000 °C, and (c) 1050 °C at region D2, and (d) plots of film coverage (red) and domain size (blue) *vs.* growth temperature.

Results and discussion

To understand the growth of h-BN in an APCVD system, we conducted a systemic study on various critical parameters, in an attempt to achieve a well-controlled h-BN film. In this report, we discussed the effects of substrate position, growth temperature (T_2), growth duration, precursor temperature (T_1), and weight of ammonia borane. One of the main disadvantages for APCVD is its non-uniform density distribution due to its operation in the mass transport limited regime. As such, the above parameters are of potential importance to synthesize high quality uniform h-BN films.

Substrate position

In our setup, h-BN film coverage as well as domain size increased downstream along the tube, away from the precursor, as depicted in Fig. 2a–f, highlighting the substrate position as an important parameter to control the film-growth and coverage. As shown in Fig. 2a–c, the growth process undergoes a

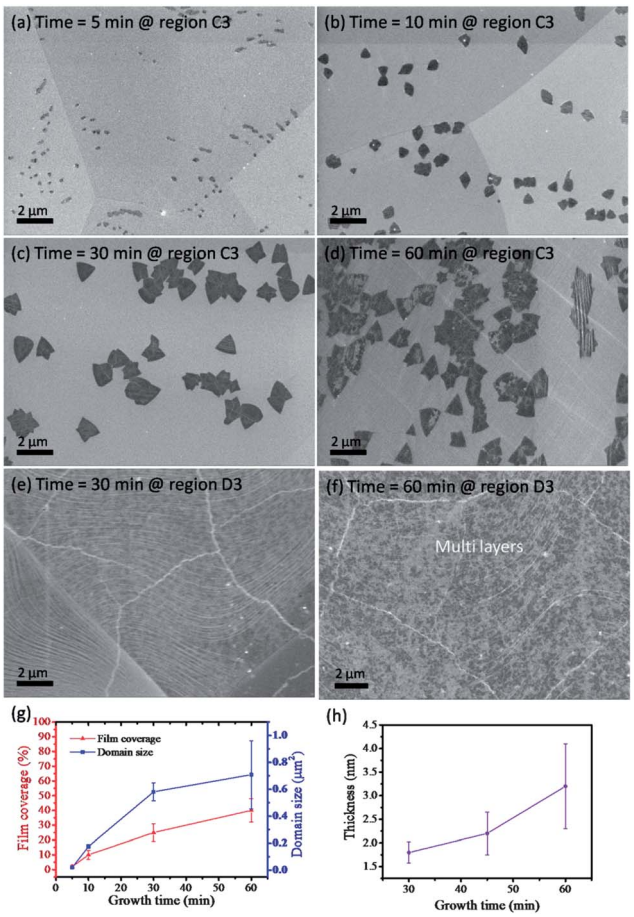

Fig. 5 Growth time dependence of h-BN films. SEM images of the as-grown h-BN on Cu with a growth time of (a) 5 min, (b) 10 min, (c) 30 min, (d) 60 min at region C3, and at (e) 30 min, and (f) 60 min at region D3. (g) Plots of film coverage (red) and domain size (blue) *vs.* growth time, and (h) a plot of film thickness *vs.* growth time.

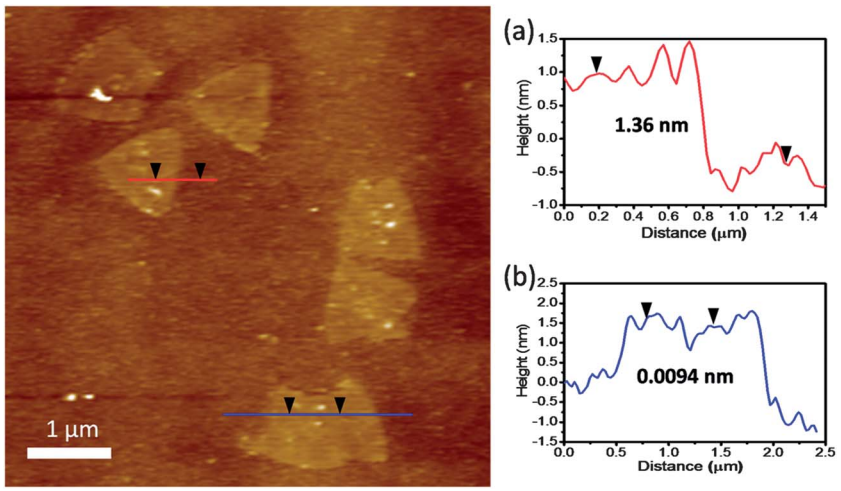

Fig. 4 AFM image of transferred triangular h-BN domains on SiO_2/Si substrate with its corresponding height profile of (a) an individual domain, and (b) conjoined h-BN domains.

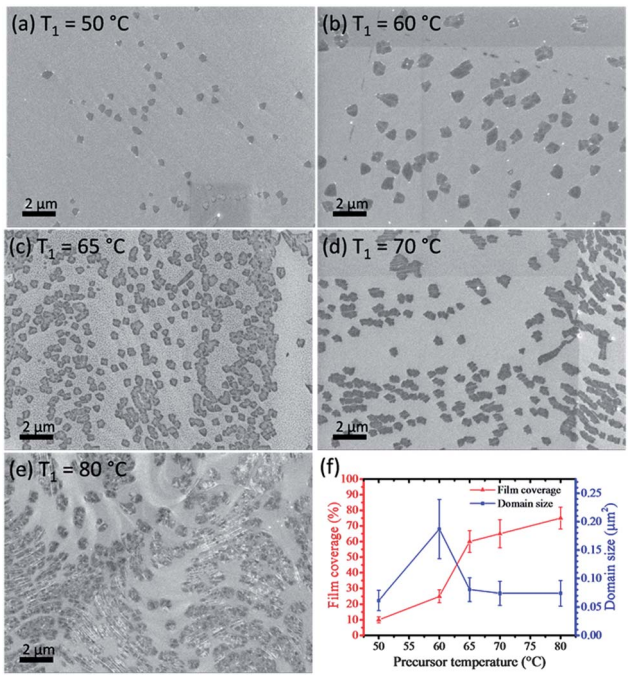

Fig. 6 Precursor temperature (T_1) dependence of h-BN domains grown for 10 min at Region C3. SEM images of the as-grown h-BN on Cu at various T_1 of (a) 50, (b) 60, (c) 65, (d) 70, and (e) 80 °C using 5 mg of ammonia borane.(f) Plot of film coverage (red) and domain sizes (blue) *vs.* precursor temperature.

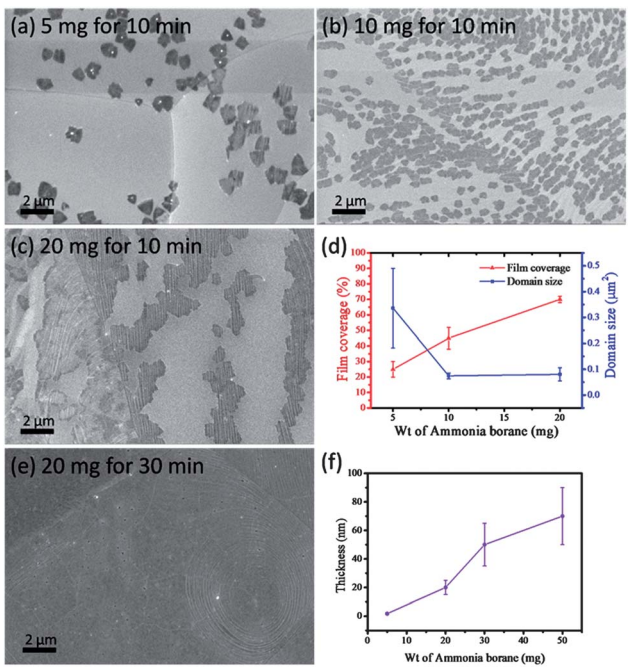

Fig. 7 Amount of ammonia borane dependence of h-BN domains at region D2. SEM images of the as-grown h-BN on Cu with different masses of the precursor (a) 5 mg, (b) 10 mg and (c) 20 mg heated at 60 °C for 10 min. (d) Plot of film coverage (red) and domain sizes (blue) *vs.* weight of ammonia borane. (e) SEM image of a thick h-BN film on Cu using 20 mg of ammonia borane and grown for 30 min. (f) plot of film thickness *vs.* weight of ammonia borane.

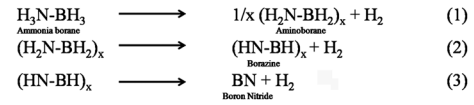

Scheme 1 Reaction processes of BN formation from the ammonia borane precursor.

dramatic change in h-BN domain size and density. The graph in Fig. 2f compares the h-BN domain size and film coverage with respect to the substrate position. Growth condition dependent evolution of domain size and density has also been observed previously in a 2D graphene material.[26] The trend of increasing in both domain density and size was also found to be consistent, even when the flow rate of the carrier gas was reduced. The rate of nucleation is affected by a combination of factors such as the temperature gradient of the gas molecules and the concentration of the active species in the tube. As cold air enters the tube, air molecules in the front region of the tube (region A) have a lower temperature and gradually heat as they move along the quartz tube (region D). Due to the increased temperature, a higher concentration of active decomposed species occurs farther from the precursor, leading to a uniform growth of film coverage. The evolution of h-BN growth at different stages is due to vapor phase dispersion of the by-products of decomposed ammonia borane. The precursor ammonia borane dehydrogenates into aminoborane (H_2NBH_2) and borazine $(HNBH)_3$ (ref. 27 and 28) when heated to 60 °C. These by-products may further decompose at higher temperatures leading to subsequent chain reactions towards the end of the tube. A similar phenomenon of increasing film density was also observed in CVD-grown graphene, due to the increase in the active species from methane cracking downstream along the quartz tube.[29]

Growth temperature

Temperature is another crucial factor for the material growth. It plays an important role to achieve high quality material in terms of its control over thickness, domain sizes, and uniformity. SEM images in Fig. 3a–c show the evolution of the h-BN domains and coverage at three different temperatures: 950 °C, 1000 °C, and 1050 °C, respectively. Noticeably, a little change (50 °C) in temperature results in a significant increase (~17-fold) in the average domain size when the growth temperature was raised from 1000 °C to 1050 °C as depicted in Fig. 3b and c, respectively. Temperature dependent evolution of domain sizes and film coverage have been presented in Fig. 3d. Higher growth temperature increases the growth rate and crystallinity, and greatly favors the lateral growth of the h-BN domains, which is essential for high quality films with larger grains.

Triangular-shaped h-BN domains

Fig. 4 shows the AFM image of the triangular h-BN flakes transferred onto the SiO_2/Si substrate. The thicknesses of the flakes were measured to be around 1.36 nm which corresponds to 2 to 3 atomic layers. It was also observed that the conjoined h-BN domains were seamlessly stitched (without overlapping)

Table 1 Factors and effects on h-BN film-growth

APCVD parameters	Effects on film-growth
Substrate position	Film density and domain sizes increase downstream along the quartz tube.
Growth temperature (T_2)	Higher temperature of above 1000 °C is favorable for high quality h-BN films.
Growth duration	Domain density, grain sizes and film thickness increase with growth time.
Precursor temperature (T_1)	Generally, a low temperature of ~60 °C is sufficient for film-growth with largest domain size. Domain sizes reduce with increasing temperature beyond 60 °C.
Amount of precursor	Domain density and film thickness increase with increasing quantity of precursor. However, domain sizes reduce.

as indicated by an almost uniform height profile within the domains. Thus, the growth is predicted to begin with a mono, bi, or even a few layers of nucleuses forming large domains. The crystalline h-BN domains adopt a triangular shape due to the asymmetric edge energy of the B-rich and N-rich sides,[30] where all three sides should be N-terminated as it is energetically more favorable. However, in contrast to the perfect triangles grown by LPCVD,[19,20] we observed the triangular domains to have slightly curved edges and occasionally rounded apexes. In APCVD, there is a non-uniform density distribution due to the irregularities in gas flow hence causing the irregular shapes.

Furthermore, the substrate property and its surface quality are known to have important effects on the growth, orientation and quality of graphene.[31,32] After annealing at high temperature, the Cu substrate grows in grain size and re-crystallizes predominantly to a (100) surface orientation. Similarly, the growth of h-BN on Ni (111) nucleates in the form of triangular islands with two different orientations where the boron atoms are bonded on either Ni hcp or fcc sites, respectively.[33] However, for h-BN on the Cu (100) surface, the h-BN triangular islands nucleate in random orientations as can be observed in our samples. The reason for the difference is due to the symmetry of the (111) surface of a fcc crystal, which is hexagonal, while the symmetry of the (100) surface is a square. h-BN domains are expected to have fewer rotational orientations on a (111) surface as compared to a (100) surface. In addition, Cu (100) has a higher lattice mis-match to h-BN than Cu (111) or Ni (111), which results in more misalignments of h-BN grains on the Cu lattice.

Deposition time

The domain sizes and film coverage can also be controlled by varying the deposition time. Fig. 5a–g shows the increase in size

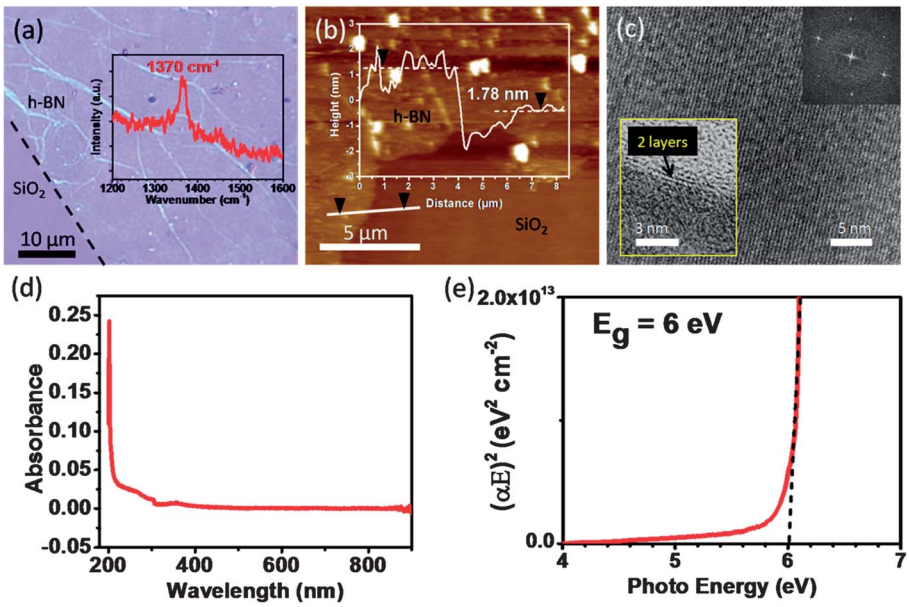

Fig. 8 Characterization of the continuous h-BN film. (a) Optical image with enhanced contrast and its corresponding Raman spectrum (inset), (b) AFM image with a plot (inset) of the thickness of a continuous h-BN film transferred onto a SiO_2/Si substrate. (c) Top-view TEM image with FFT (inset) showing the hexagonal structure, and cross-section TEM (inset) consisting of the bilayer h-BN film. (d) Ultraviolet-visible absorption spectrum of the h-BN film at room temperature and (e) $(\alpha E)^2$ *vs.* E plot for bandgap measurement.

and film coverage of h-BN on region C3 at 5, 10, 30 and 60 min, respectively. However, the film became continuous on D3 when the precursor was heated beyond 30 min. Fig. 5e and f show the progression of film coverage with an increasing number of layers of film on region D3 at 30 and 60 min, respectively, which clearly shows that the growth of the h-BN film on Cu substrates is not self-limited. This trend in film growth was not observed until around 30 min of deposition time (at region D), and before that, it remained sporadic with triangular domains. Thickness of the continuous film *vs.* deposition time is presented in Fig. 5h.

After a longer growth time, the film grows in thickness, this could possibly be because the growth mode follows the combination of a layer-by-layer growth and island growth (Stranski–Krastanov growth).[34] A transition from layer-by-layer growth to island growth occurs at a critical thickness, depending on the chemical and physical properties of the substrate and of the film, such as surface energies and lattice parameters. In our study, based on the relatively high thickness uniformity and the lower surface roughness of the h-BN film (measured using AFM), we may consider a thickness of ~1.8 nm (3 or 4 layers of h-BN) to be a critical thickness. Following this growth mode, under a longer growth time, the film grows laterally as well as vertically resulting in a multilayer film with enhanced roughness. An increase in the thickness (presented in Fig. 5h) and surface roughness of the h-BN film with growth time is evident from our AFM measurements (Fig. 8b).

Precursor

The temperature at T_1 was varied from 50 °C to 80 °C (±5 °C) using a fixed amount (5 mg) of ammonia borane (Fig. 6). The significantly smaller domain size with low density at 50 °C was due to the lack of active precursors. When the temperature was raised to 60 °C, the largest domain size was observed but decreased as the temperature further increased. However, significantly more nucleation sites were formed, thus increasing the film coverage (Fig. 6f). This result stands in agreement with the recent report by Gao *et al.*[21] which describes the same phenomenon of the growth of h-BN on platinum foil under APCVD conditions.

At 60 °C, polymeric aminoborane dehydrogenates and breaks into hydrogen (H_2), aminoborane (H_2NBH_2) and borazine $(HNBH)_3$.[27,28] As such, an increase in temperature would favour the promotion of the rate of decomposition and hence the nucleation. Similarly, by increasing the amount of the ammonia borane precursor, the density of the h-BN domains also increases significantly as shown in Fig. 7a–c. As more ammonia borane is used, higher amounts of decomposed products are formed, leading to an increase in the number of nucleation sites. However, the domain sizes did not become larger with increasing amounts of precursor. On the contrary, the domains reduced in size as plotted in Fig. 7d. This shows that increasing the amount of precursor favours nucleation, but not the growth of grain sizes. Nonetheless, it is necessary to increase the quantity of ammonia borane in order to achieve thicker layers of h-BN film. Fig. 7e shows an SEM image of a thick h-BN film on a Cu substrate using 20 mg of ammonia borane and grown for 30 min. The plot of film thickness *vs.* amount of ammonia borane is presented in Fig. 7f. Due to the abundance of ammonia borane, and without any self-limiting growth of h-BN, the film thickness grows with an extended growth time of 30 min.

A possible CVD-growth mechanism for the h-BN film using ammonia borane as precursor is illustrated in Scheme 1. First, thermal decomposition of ammonia borane produces aminoborane (1) and borazine molecules (2). At high growth temperature, the hydrogen atoms dissociate leaving behind active BN species (3). The hydrogen atoms recombine to form hydrogen molecules that are transported away while the active BN diffuses on the Cu surface. Nucleation occurs on the Cu surface and the active BN species are attached and bonded along the nucleuses or along the growing edges of the triangular domains.

The conclusive remarks of the above discussions are presented in Table 1.

The full coverage h-BN thin films were subsequently transferred onto SiO_2/Si and quartz substrates for further characterization. Fig. 8a shows an optical image of a continuous h-BN film transferred onto a SiO_2/Si substrate. Characteristic wrinkles are observed due to the PMMA transfer process. There is a Raman peak located at 1370 cm^{-1} (inset of Fig. 8a), which confirms the presence of the h-BN film, as the Raman peak corresponds to the E_{2g} vibration mode of h-BN.[35] The AFM image, taken at the edge of the h-BN film, measures at around 1.78 nm thick, as shown in Fig. 8b. The TEM image in Fig. 8c shows the crystalline h-BN film with its corresponding fast Fourier transform (FFT) (inset of Fig. 8c), revealing a distinct hexagonal structure, and the cross-section TEM (inset of Fig. 8c) shows the presence of a bilayer h-BN film. In order to measure its optical bandgap (OBG), the h-BN film was transferred onto a quartz substrate and the UV-visible absorption spectrum was carried out using an identical blank quartz substrate as a reference for baseline measurements. Fig. 8d shows the absorption spectrum of a highly transparent h-BN thin film with a sharp peak at 202 nm. For a direct bandgap semiconductor, h-BN, the derived formula to calculate its OBG is given by its absorption coefficient, $\alpha = C(E - E_g)^{1/2}/E$.[36] Where $\alpha = A/d$ (A is the optical absorption measured by the UV-visible spectroscopy and d is the thickness of the film), C is a constant and E, the photo energy, is calculated by $E = hc/\lambda$ where h is Plank's constant, and λ is the wavelength. Following this equation, we should obtain a straight line when we plot $(\alpha E)^2$ *vs.* E in Fig. 8e. Thus, by extrapolation of the straight line part of the curve, the intersection point of the straight line and the x-axis, when $(\alpha E)^2 = 0$, corresponds to the estimated value of the bandgap, E_g. Here, we used 1.78 nm as the film thickness as measured by AFM and obtained a bandgap of 6 eV. The high bandgap indicates that the h-BN film is electrically non-conductive and correlates well to the theoretical value of monolayer h-BN.[37] These results conclude that our h-BN films synthesized through this method consist of a monolayer to a few layers, and they are transparent and electrically non-conductive with a high bandgap of 6 eV.

Conclusions

In summary, we have demonstrated a systematic approach of controlling the growth of h-BN film by APCVD on copper substrates. The breakdown of the effects of film-growth due to different CVD parameters has been described in Table 1. Being subjected to factors such as temperature gradient and gas flow dynamics, the concentration of active species along the quartz tube increased downstream, causing a non-uniform distribution of density at different regions of the quartz tube. Due to these factors, an increasing gradient of film coverage was observed along the substrate. For a slight increase in temperature of 50 °C (1000 °C to 1050 °C), we observed a significant (~17-fold) increase in average domain size, and it further increased for longer time of growth. The h-BN flakes nucleated in the form of triangles and coalesced between adjacent domains. The clusters continued to grow and eventually formed a continuous film. In order to have a good control of domain size, film coverage and thickness, it is also important to tune the precursor parameters such as temperature and the amount of ammonia borane. In contrast with previously mentioned factors (substrate position, growth temperature and time), the effect of precursor is slightly more complex. A significant increase in nucleation was observed when higher temperature (T_1) or greater amounts of ammonia borane was used. However, the triangular domains notably were reduced in size. This shows that a higher amount of active decomposed species favours more nucleation rather than grain growth. However, in order to achieve thicker films, besides increasing deposition time, a higher quantity of ammonia borane is required. h-BN films synthesized in this work are crystalline, highly transparent and electrically non-conducting with a high bandgap of 6 eV. APCVD is a simple yet efficient method to produce high quality h-BN films which can be employed in mass production. It effectively reduces the use of additional resources and complications of copper evaporation. However, non-uniformity still remains an issue, especially for large scale synthesis, which can be corrected by optimizing the substrate position and gas flow rate. A technique used to overcome this for large scale deposition is by increasing the flow rate of the precursor by gradual increments to target different regions of growth on the substrate.[38]

Acknowledgements

The authors acknowledge the support from MINDEF Singapore and the Army Research Laboratory (ARL), USA. The authors would also like to thank Prof. Pulickel M. Ajayan of Rice University, Dr Shashi P. Karna and Dr Mark Griep of ARL for their valuable input and suggestions.

Notes and references

1 K. Watanabe, T. Taniguchi and H. Kanda, *Nat. Mater.*, 2004, **3**, 404–409.
2 A. Lipp, K. A. Schwetz and K. Hunold, *J. Eur. Ceram. Soc.*, 1989, **5**, 3–9.
3 O. Tao, C. Yuanping, X. Yuee, Y. Kaike, B. Zhigang and Z. Jianxin, *Nanotechnology*, 2010, **21**, 245701.
4 C. R. Dean, A. F. Young, I. Meric, C. Lee, L. Wang, S. Sorgenfrei, K. Watanabe, T. Taniguchi, P. Kim, K. L. Shepard and J. Hone, *Nat. Nanotechnol.*, 2010, **5**, 722–726.
5 K. K. Kim, A. Hsu, X. Jia, S. M. Kim, Y. Shi, M. Dresselhaus, T. Palacios and J. Kong, *ACS Nano*, 2012, **6**, 8583–8590.
6 K. H. Lee, H.-J. Shin, J. Lee, I.-Y. Lee, G.-H. Kim, J.-Y. Choi and S.-W. Kim, *Nano Lett.*, 2012, **12**, 714–718.
7 W. Auwarter, T. J. Kreutz, T. Greber and J. Osterwalder, *Surf. Sci.*, 1999, **429**, 229–236.
8 E. Husain, T. N. Narayanan, J. J. Taha-Tijerina, S. Vinod, R. Vajtai and P. M. Ajayan, *ACS Appl. Mater. Interfaces*, 2013, **5**, 4129–4135.
9 Z. Liu, Y. Gong, W. Zhou, L. Ma, J. Yu, J. C. Idrobo, J. Jung, A. H. MacDonald, R. Vajtai, J. Lou and P. M. Ajayan, *Nat. Commun.*, 2013, **4**, 2541.
10 T. Fujihara, H.-B. Cho, T. Nakayama, T. Suzuki, W. Jiang, H. Suematsu, H. D. Kim and K. Niihara, *J. Am. Ceram. Soc.*, 2012, **95**, 369–373.
11 L. Britnell, R. V. Gorbachev, R. Jalil, B. D. Belle, F. Schedin, A. Mishchenko, T. Georgiou, M. I. Katsnelson, L. Eaves, S. V. Morozov, N. M. R. Peres, J. Leist, A. K. Geim, K. S. Novoselov and L. A. Ponomarenko, *Science*, 2012, **335**, 947–950.
12 T. P. Brennan, J. R. Bakke, I. K. Ding, B. E. Hardin, W. H. Nguyen, R. Mondal, C. D. Bailie, G. Y. Margulis, E. T. Hoke, A. Sellinger, M. D. McGehee and S. F. Bent, *Phys. Chem. Chem. Phys.*, 2012, **14**, 12130–12140.
13 J. R. Bakke, K. L. Pickrahn, T. P. Brennan and S. F. Bent, *Nanoscale*, 2011, **3**, 3482–3508.
14 D. Pacile, J. C. Meyer, C. O. Girit and A. Zettl, *Appl. Phys. Lett.*, 2008, **92**, 133107.
15 L. H. Li, Y. Chen, G. Behan, H. Zhang, M. Petravic and A. M. Glushenkov, *J. Mater. Chem.*, 2011, **21**, 11862–11866.
16 J. N. Coleman, M. Lotya, A. O'Neill, S. D. Bergin, P. J. King, U. Khan, K. Young, A. Gaucher, S. De, R. J. Smith, I. V. Shvets, S. K. Arora, G. Stanton, K. Hye-Young, L. Kangho, G. T. Kim, G. S. Duesberg, T. Hallam, J. J. Boland, W. Jing Jing, J. F. Donegan, J. C. Grunlan, G. Moriarty, A. Shmeliov, R. J. Nicholls, J. M. Perkins, E. M. Grieveson, K. Theuwissen, D. W. McComb, P. D. Nellist and V. Nicolosi, *Science*, 2011, **331**, 568–571.
17 Y. Lin, T. V. Williams and J. W. Connell, *J. Phys. Chem. Lett.*, 2010, **1**, 277–283.
18 L. Song, L. Ci, H. Lu, P. B. Sorokin, C. Jin, J. Ni, A. G. Kvashnin, D. G. Kvashnin, J. Lou, B. I. Yakobson and P. M. Ajayan, *Nano Lett.*, 2010, **10**, 3209–3215.
19 K. K. Kim, A. Hsu, X. Jia, S. M. Kim, Y. Shi, M. Hofmann, D. Nezich, J. F. Rodriguez-Nieva, M. Dresselhaus, T. Palacios and J. Kong, *Nano Lett.*, 2012, **12**, 161–166.
20 N. Guo, J. Wei, L. Fan, Y. Jia, D. Liang, H. Zhu, K. Wang and D. Wu, *Nanotechnology*, 2012, **23**, 415605.
21 Y. Gao, W. Ren, T. Ma, Z. Liu, Y. Zhang, W.-B. Liu, L.-P. Ma, X. Ma and H.-M. Cheng, *ACS Nano*, 2013, **7**, 5199–5206.

22 G. Kim, A. R. Jang, H. Y. Jeong, Z. Lee, D. J. Kang and H. S. Shin, *Nano Lett.*, 2013, **13**, 1834–1839.
23 A. Ismach, H. Chou, D. A. Ferrer, Y. Wu, S. McDonnell, H. C. Floresca, A. Covacevich, C. Pope, R. Piner, M. J. Kim, R. M. Wallace, L. Colombo and R. S. Ruoff, *ACS Nano*, 2012, **6**, 6378–6385.
24 A. J. Melmed and K. B. Keating, *Surf. Sci.*, 1966, **5**, 166–169.
25 X. Li, Y. Zhu, W. Cai, M. Borysiak, B. Han, D. Chen, R. D. Piner, L. Colomba and R. S. Ruoff, *Nano Lett.*, 2009, **9**, 4359–4363.
26 L. Liu, H. Zhou, R. Cheng, Y. Chen, Y.-C. Lin, Y. Qu, J. Bai, I. A. Ivanov, G. Liu, Y. Huang and X. Duan, *J. Mater. Chem.*, 2012, **22**, 1498–1503.
27 F. Baitalow, G. Wolf, J. P. E. Grolier, F. Dan and S. L. Randzio, *Thermochim. Acta*, 2006, **445**, 121–125.
28 J. Baumann, F. Baitalow and G. Wolf, *Thermochim. Acta*, 2005, **430**, 9–14.
29 Z. Li, W. Zhang, X. Fan, P. Wu, C. Zeng, Z. Li, X. Zhai, J. Yang and J. Hou, *J. Phys. Chem. C*, 2012, **116**, 10557–10562.
30 Y. Liu, S. Bhowmick and B. I. Yakobson, *Nano Lett.*, 2011, **11**, 3113–3116.
31 Z. R. Robinson, P. Tyagi, T. M. Murray, C. A. Ventrice, Jr, C. Shanshan, A. Munson, C. W. Magnuson and R. S. Ruoff, *J. Vac. Sci. Technol., A*, 2012, **30**, 011401.
32 L. Zhao, K. T. Rim, H. Zhou, R. He, T. F. Heinz, A. Pinczuk, G. W. Flynn and A. N. Pasupathy, *Solid State Commun.*, 2011, **151**, 509–513.
33 W. Auwarter, M. Muntwiler, J. Osterwalder and T. Greber, *Surf. Sci.*, 2003, **545**, 735–740.
34 J. A. Venables, *Introduction to Surface and Thin Film Processes [electronic resource]*, Cambridge, Cambridge University Press, 2000.
35 R. V. Gorbachev, I. Riaz, R. R. Nair, R. Jalil, L. Britnell, B. D. Belle, E. W. Hill, K. S. Novoselov, K. Watanabe, T. Taniguchi, A. K. Geim and P. Blake, *Small*, 2011, **7**, 465–468.
36 T. H. Yuzuriha and D. W. Hess, *Thin Solid Films*, 1986, **140**, 199–207.
37 X. Blase, A. Rubio, S. G. Louie and M. L. Cohen, *Phys. Rev. B: Condens. Matter Mater. Phys.*, 1995, **51**, 6868–6875.
38 I. Vlassiouk, P. Fulvio, H. Meyer, N. Lavrik, S. Dai, P. Datskos and S. Smirnov, *Carbon*, 2013, **54**, 58–67.